AIAA JOURNAL
Vol. 38, No. 11, November 2000

Numerical Simulation of Shock-Enhanced Mixing in Nonuniform Density Turbulent Jets

Shigeo Obata*
National Defense Academy, Yokosuka, Kanagawa 239-8686, Japan
and
James C. Hermanson†
Worcester Polytechnic Institute, Worcester, Massachusetts 01609-2280

A numerical study of the interaction of weak normal shock waves with turbulent jets was conducted. The configuration consisted of a planar jet of air, helium, or carbon dioxide situated on the centerline of a shock tube with an air coflow. The shock strengths were $M_s = 1.2$ and 1.4. The numerical model was based on a time-dependent, Navier–Stokes approach and a two-equation q–ω turbulence model. The results indicate that passage of a shock through low-density (helium) jets produces a vortexlike structure not seen for the case of the air or carbon dioxide jets. Helium jets exhibit a decrease in mean jet fluid concentration due to shock interaction of up to approximately 30% at a location 30 jet exit heights downstream of the jet exit for a shock strength of $M_s = 1.4$. The amount of mixing enhancement increases with increasing shock strength and decreases with increasing downstream distance. In comparison, the air and carbon dioxide jets show a significantly smaller degree of mixing enhancement. These results are qualitatively consistent with recent experimental results in axisymmetric, turbulent jets subject to normal shock passage.

Introduction

ATTAINING very rapid and efficient mixing in compressible jet flows is crucial to the successful implementation of supersonic combustion devices, given the very short residence time in the combustor. Mixing improvement in supersonic shear flows is, thus, a subject of continuing interest in fluid mechanics and combustion communities. One topic of fundamental interest is the interaction of shocks with turbulent jets and the consequent shock-induced mixing augmentation and changes in turbulent jet structure. This problem is of direct importance to supersonic combustion applications, given the inevitability of shock waves and regions of nonuniform density in a scramjet combustor.

Although the penetration and mixing characteristics of gas jets issuing into supersonic primary streams have been examined previously, for example, by Hollo et al.[1] and Hermanson and Winter,[2] the features of the interaction of these jets with compression waves, such as changes in jet structure and mixing rate, are not fully established. Previous work[3,4] has suggested that mixing enhancement in fuel jets can be brought about by the baroclinic vorticity generated by the shock/jet interaction. Strong, nonuniform acceleration can also lead to shear (Kelvin–Helmholtz) and inertial (Rayleigh–Taylor) instability.[5–7] Thus, the growth of actual disturbances and subsequent mixing enhancement may be a combined result of several instability mechanisms to an extent as yet not fully established.

Several flow configurations have been studied experimentally and numerically to examine the effectiveness of baroclinic vorticity and other shock-induced mixing enhancement mechanisms. For example, the investigation of the behavior of spherical and cylindrical regions of different density on passage of normal shock waves has provided a clear demonstration of vorticity generation by the baroclinic effect.[6] Many of the previous studies of the interaction of vortical structures with shock waves,[8–12] have focused more on the noise production than on mixing enhancement. The mixing enhancement and flow structure for this problem were studied experimentally by Cetegen and Hermanson.[7] Numerical and analytical studies were conducted for similar shock wave/vortex interactions by Ellzey et al.[13] The passage of shock waves in free turbulence has also been studied experimentally[14] and computationally[15] and has demonstrated the creation of high-intensity Reynolds stresses and increased turbulence due to shock passage.

The interaction of propagating shock waves with laminar jets has also been studied in experiments and by numerical simulations.[16–19] Jacobs[18] investigated the interaction of a normal shock wave propagating over the cross section of a laminar helium jet. The dynamics of the vorticity production due to shock interaction was seen to result in the generation of a vortex pair. Quantitative information on the degree of mixing enhancement in a similar configuration was reported by Budzinski.[19]

Huh and Driscoll[20] examined the interaction of oblique shocks with a nonpremixed, supersonic flame and report an increase in fuel/air mixing that resulted in a decrease in the flame length by as much as 20%. The case of shock interactions with a turbulent gas jet has also recently been studied by Hermanson and Cetegen.[21,22] They studied experimentally the mixing enhancement in an axisymmetric turbulent jet of nonuniform density caused by the passage of weak shock waves along the jet axis. This is a configuration of practical interest that extended the previous studies in laminar jets, vortex rings, and stagnant gas regions by bringing in the important effects of turbulence and the associated rapid mixing and dilution. The simplicity of this configuration aids in the study of the fundamental mixing mechanisms operative in more complicated combustor geometries. Previous work[3,4] has demonstrated the utility of using unsteady shock propagation to study mixing processes in compressible jet flows by showing that the intersection of an oblique shock wave with a steady fuel jet can be simulated, locally, by the passage of a shock wave though a stationary cylindrical region of gas.

Experiments for the case of weak normal shocks interacting with light gas turbulent jets (helium jets in air) have shown the generation of a pronounced secondary vortex structure.[21,22] There also appeared to be a clear reduction in mean fluid concentration caused by shock passage, indicating an increased rate of dilution and mixing. Neither the structural change or a measurable impact on mixing was apparent for constant density jets. In addition, such changes were also not apparent for a heavy jet (carbon dioxide into air) even though the mean magnitude of the density gradient was comparable to that for the light jets at the same shock strength.[22]

In this paper we report complementary numerical results on mixing enhancement caused by the passage of weak shock waves along

Received 1 September 1999; revision received 20 April 2000; accepted for publication 25 April 2000.

*Lecturer, AeroSpace Engineering Department, 1-10-20 Hashirimizu; obata@cc.nda.ac.jp.

†Associate Professor, Mechanical Engineering Department, 100 Institute Road; jherm@wpi.edu. Associate Fellow AIAA.

the axis of planar, turbulent jets of nonuniform density. The numerical model is based on a time-dependent, Navier–Stokes (N–S) approach and employs a two-equation turbulent (q–ω) model for the modeling of turbulent transport. The two primary experimental variables are the density ratio between the jet gas and the surrounding airstream and the shock strength.

Numerical Simulation Approach

The time-dependent conservation equations (mass, N–S, and energy), coupled with a multi-species conservation and turbulence model, were adopted as the governing equations for the numerical modeling of the changes in turbulent mixing due to shock passage. All principal physical quantities, such as density and pressure, temperature, and velocity, were represented in these equations. The two-equation turbulent (q–ω) model by Coakley[23] was employed for the modeling of turbulent transport. Transport variables, such as molecular diffusivity, viscosity, and thermal conductivity were expressed as the sum of laminar and turbulent values. The laminar transport coefficients were estimated from the molecular collision constants; those for turbulent transport were obtained from the two-equation turbulent model.

The basic computational flow properties, the density ρ, velocity $\boldsymbol{U}$, and total energy e are contained in the three conservation equations for mass, momentum, and energy shown here:

$$\dot{\rho} + \nabla \cdot \rho \boldsymbol{U} = 0 \tag{1}$$

$$\rho \dot{\boldsymbol{U}} + \boldsymbol{U} \nabla \cdot \rho \boldsymbol{U} = \nabla \cdot \boldsymbol{\sigma} \tag{2}$$

$$\rho \dot{e} + \nabla \cdot \rho (e + p) \boldsymbol{U} = \nabla \cdot (\boldsymbol{U} \cdot \boldsymbol{\sigma}) - \nabla \cdot \boldsymbol{K} \tag{3}$$

where an overdot indicates a time derivative, $\boldsymbol{\sigma}$ is the flow stress tensor, and $\boldsymbol{K}$ is an energy flux vector. The conservation equation for the chemical species is represented by a species mole density f_k:

$$\dot{f}_k + \nabla \cdot f_k U = -\nabla \cdot \boldsymbol{J} \tag{4}$$

where the diffusion coefficient $\boldsymbol{J}$ represents the sum of the laminar and turbulent diffusion processes.

The modeling of the turbulent viscosity is central to the numerical simulation. The two-equation q–ω turbulence model employed in this work was chosen largely for its generally excellent numerical stability. A turbulent velocity scale q and a turbulent frequency scale ω are the principal variables in the model. These two parameters are governed by the two equations for turbulent energy conservation and turbulent dissipation conservation:

$$\rho \dot{q} + \nabla \cdot \rho q \boldsymbol{U} = \nabla \cdot \boldsymbol{G}_q + H_q \tag{5}$$

$$\rho \dot{\omega} + \nabla \cdot \rho \omega \boldsymbol{U} = \nabla \cdot \boldsymbol{G}_\omega + H_\omega \tag{6}$$

where $\boldsymbol{G}$ and H, respectively, indicate the viscous dissipation terms and the production source terms. Here, q and ω were used to compute the turbulent viscosity used in the definition of $\boldsymbol{G}$. The source terms H were defined in terms of the flow stress as determined from the velocity, as explained in Ref. 23. The values of q and ω at the jet exit were determined from the experimental planar jet results of Gutmark and Wygnanski.[24]

The numerical scheme was based on a lower–upper alternating direction implicit (LU-ADI) approximate factorization total variation diminishing (TVD) finite difference formulation of full N–S equation by Obayashi et al.[25] The discretization is first order in time and third order in accuracy for the convective terms according to the Chakravarthy and Osher[26] upwind TVD formulation, and second order for central-differenced viscous diffusion terms. Good convergence was attained by employing the Van Leer-type differential flux limiter used by Anderson et al.[27] in the TVD scheme and Newton-iterative correction for the time integration.

Computational Grid and Flow Conditions

The flow conditions in these simulations were chosen to correspond, to the extent possible, to those of the experiments of Hermanson and Cetegen.[22] Those experiments were conducted using a circular jet nozzle 1.1 mm in diameter situated on the centerline of a square shock tube duct 50 × 50 mm in cross section. In the two-dimensional numerical simulations presented here, the duct half-height was 50 mm and the jet half-height 0.55 mm. Computations were performed on a grid consisting of 115 points in the downstream direction and 25 points in the transverse direction. The downstream distance, normalized by the nozzle full-height, ranged from $x/h = -32$ to 59.

The jet exit velocities were taken to be $U_0 = 206$ m/s for the air jet, $U_0 = 531$ m/s for the helium jet, and $U_0 = 193$ m/s for the carbon dioxide jet. The corresponding jet Reynolds numbers, based on the full nozzle height and the velocity and kinematic viscosity of the injected gas were $Re_0 = 10{,}700$; 3,700; and 18,800 for the air, helium, and carbon dioxide jets, respectively. These are comparable to the injection Reynolds numbers used by Hermanson and Cetegen.[22] The rationale for the different values lies in the fact that the local Reynolds number, defined as $Re_d = U_{cl}\delta/\nu_{cl}$, where U_{cl} is the mean centerline velocity, δ the local jet width, and ν_{cl} the kinematic viscosity corresponding to the mean centerline composition, changes with downstream distance owing to the dilution of the jet with air. This results in an increase in Reynolds number for the helium jet and a corresponding decrease for the carbon dioxide jet, allowing the study of shock-enhanced mixing in regions of comparable local Reynolds number. The temperature of the jet at the nozzle exit was in all cases 350 K; the temperature of the coflow was 300 K. The strength of the air coflow for the two-dimensional numerical simulations reported here was determined by matching the ratio of the jet momentum to that of the coflow ($\rho_0 U_0^2 A_0/\rho_{air} U_{air}^2 A_{air}$) with that from the experiments of Hermanson and Cetegen.[22] Here A_0 and A_{air} are the cross-sectional areas of the jet exit and coflow duct, respectively. This gave an air coflow velocity of 6.5 m/s for the air and carbon dioxide jets and 11.0 m/s for the helium jet. The air coflow velocity was sufficiently high in all cases to prevent jet fluid circulation within the computational domain.

The computational boundary conditions applied were as follows. At the lower boundary of the computational domain, which corresponds to the flow duct centerline, flow symmetry was enforced. The upper boundary was taken to be open and allowed the inflow of additional coflow air into the computational region due to jet entrainment. The conditions at the jet nozzle exit (pressure, temperature, density, and velocity) were fixed. In addition, the turbulent velocity parameter q and the turbulent frequency parameter ω were fixed at the nozzle exit. Both of the turbulent parameters were estimated based on 0.2 times the mean velocity and flow duct height.[24] The pressure at the coflow inlet and the computational domain outlet were fixed at the same value as at the jet exit (1 atm).

The computed average total variation over all grid points was approximately 0.1%. The total variation was defined as the average normalized sum of the variation of all flow variables (density, velocity, energy, coflow and jet species concentration, and turbulent variables) at each grid point. The stability of the computation was indicated by a Courant–Friedrichs–Lewy (CFL) number typically less than 0.5. Therefore, the absolute total error associated with each time step, equal to the product of the CFL number and the total variation, was less than 0.05%; the average error for each of the nine flow variables was 0.006%. Note that the focus of this work was not the detailed modeling of the behavior of the turbulent planar jet, but rather on the changes in jet behavior, by the use of a given turbulence model and computational approach, brought about by the passage of a normal shock wave.

Results

Steady Turbulent Jets

The concentration fields associated with planar, turbulent jets of air, helium, and carbon dioxide are shown in Figs. 1a–1c. The flow is from left to right in all cases and the entire computational domain is shown. The lines of constant concentration shown here (and in subsequent figures) are presented in increments of 0.05, with the outer edge corresponding to 5% jet fluid concentration. That the growth rate of the helium jet exceeds that of the air jet is apparent

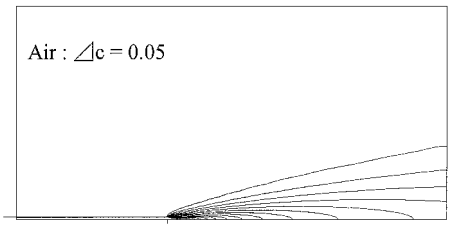

a) Air jet

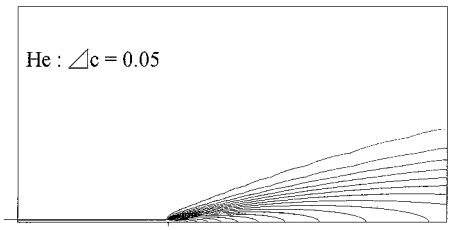

b) Helium jet

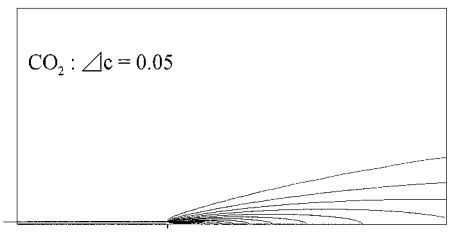

c) Carbon dioxide jet

Fig. 1 Mean concentration contours for baseline turbulent, planar jets.

from Fig. 1. The carbon dioxide jet exhibits a still lower growth rate than the air jet. These results are in qualitative agreement with previous results for planar jets.[28]

Shock/Turbulent Jet Interaction

The pressure and concentration fields of a planar, turbulent air jet undergoing the passage of an $M_s = 1.2$ shock wave are shown in Figs. 2a–2d. The corresponding pressure rise is $p_2/p_1 = 1.5$. The lines of constant pressure shown in Figs. 2a and 2c (and subsequent figures) are presented in increments of 0.1 atm. The shock propagates in all cases in the same direction as the jet flow, left to right. In Figs. 2a and 2b, the shock location is at a downstream location of $x/h = 29.6$. The corresponding location for Figs. 2c and 2d is $x/h = 53.2$. These two downstream distances are the same for all cases presented in this paper.

Subsequent to the passage of the shock wave, the jet near the nozzle region undergoes a pinching off due to the reduction in jet flow brought about by the rise in static pressure due to shock passage. The high convection velocity downstream of the shock (here ≈ 112 m/s) also shifts the jet fluid downstream of the nozzle tip, leading to the regions relatively clear of jet fluid seen in the figures. These results are qualitatively consistent with experiment.[22] Other than this, there appears to be little qualitative change in the structure of the air jet, as indicated by the mean concentration contours shown in Figs. 2b and 2d, due to the passage of the shock wave. The apparent increase in the angle of the jet with shock passage, as seen by comparing Figs. 2b and 2d with Fig. 1a, does not necessarily represent an increase in the jet growth rate. Most of the apparent change in the angle of the jet is due to convection downstream of the shock wave, with the fluid nearest the nozzle exit being displaced further downstream than fluid near the shock front at the instant in question. This shortening has important implications for the determination of the mixing enhancement of turbulent jets due to shock passage, as discussed in the following section.

Similar results are observed for the case of an air jet with a higher shock strength, $M_s = 1.4$, as shown in Figs. 3a–3d. The corresponding pressure rise is $p_2/p_1 = 2.1$. The more complete stopping of the jet flow and the greater downstream shift of the jet fluid due to shock passage are consistent with the higher static pressure rise and

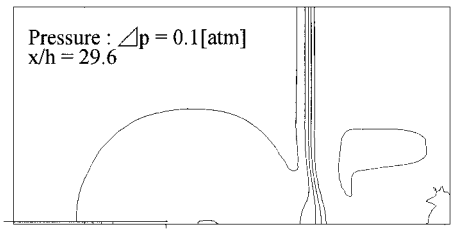

a)

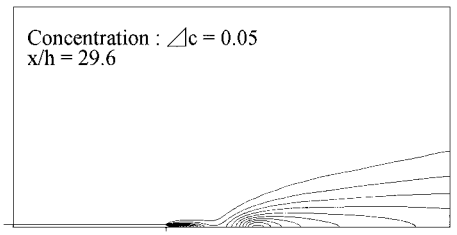

b)

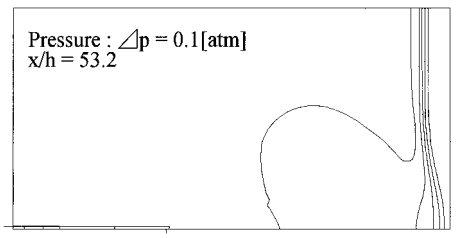

c)

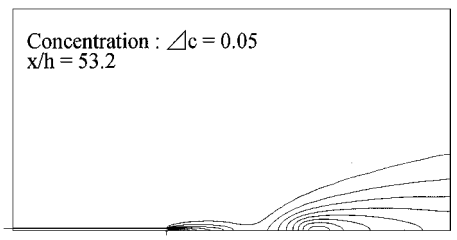

d)

Fig. 2 Pressure and concentration contours for the interaction of a normal shock wave with a turbulent air jet; shock propagation is from left to right with strength $M_s = 1.2$.

convection velocity of the gas after shock passage compared with the previous case of $M_s = 1.2$ (Figs. 2a–2d).

Corresponding results for the turbulent helium jet with shock passage are shown in Figs. 4a–4d and 5a–5d for shock waves of $M_s = 1.2$ and 1.4, respectively. The helium jet exhibits similar pinching off and convective shifting of the jet fluid due to shock passage as for the case of the air jets presented earlier. However, two effects are apparent that do not occur for the air jet. First, from the pressure contours associated with the shock wave in Figs. 4a and 4c and 5a and 5c it can be seen that the shock wave propagates slightly faster through the helium jet than through the air coflow due to the slightly higher sound speed within the jet. More strikingly, the mean concentration contours shown in Figs. 4b and 4d and 5b and 5d reveal a change in jet structure due to shock passage. The passage of the shock appears to give rise to a vortical region in the jet fluid for the case of a helium jet that does not occur for the nearly constant-density air jet. This change in structure may be a manifestation of the production of baroclinic vorticity in the out-of-plane direction, with the potential benefit of enhancing mixing between the jet fluid and its surroundings immediately behind the shock wave. The vortical structure observed for the helium jet with the weaker shock strength ($M_s = 1.2$, Figs. 4b and 4d) appears to be somewhat weaker than for the stronger $M_s = 1.4$ shock (Figs. 5b and 5d).

Corresponding concentration and pressure fields for the turbulent carbon dioxide jet with shock passage are shown in Figs. 6a–6d and

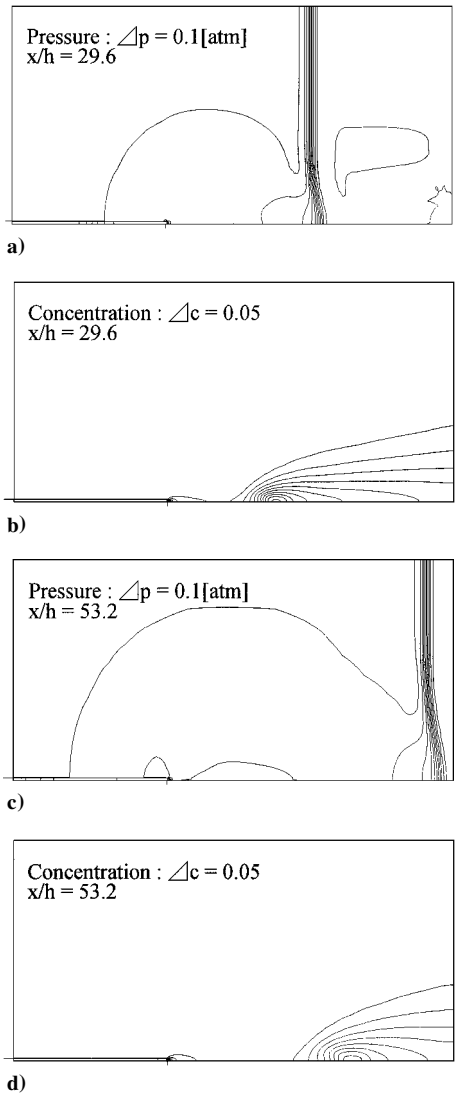

Fig. 3 Pressure and concentration contours for the interaction of a normal shock wave with a turbulent air jet; shock propagation is from left to right with strength $M_s = 1.4$.

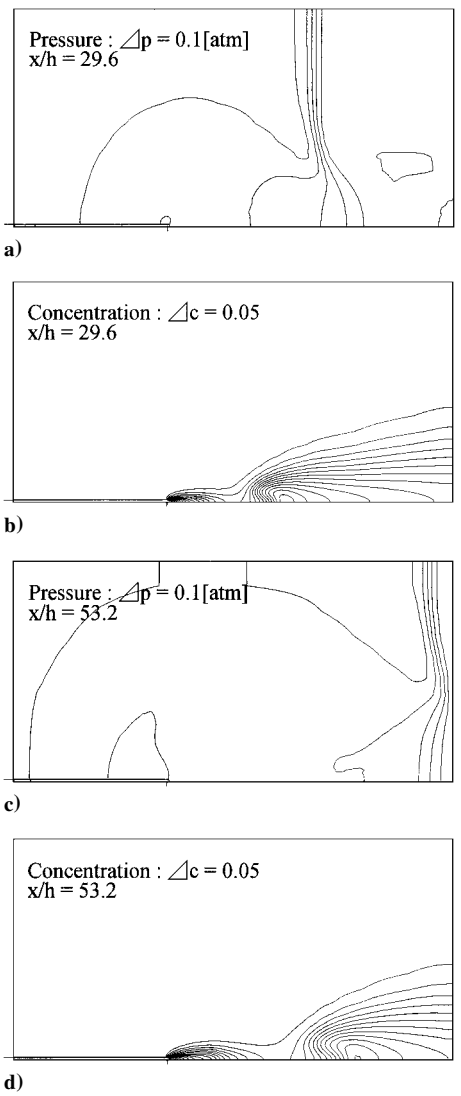

Fig. 4 Pressure and concentration contours for the interaction of a normal shock wave with a turbulent helium jet; shock propagation is from left to right with strength $M_s = 1.2$.

7a–7d, for $M_s = 1.2$ and for an $M_s = 1.4$ shock wave, respectively. The results appear qualitatively very similar to the air jet results presented earlier, but are different from those of the helium jets.

The lack of significant density gradients in the transverse direction in the air jets precludes the generation of significant amounts of the baroclinic torque believed responsible for the observed vortical structure in the case of the helium jet. In addition, that such a change in turbulent structure is not apparent for the carbon dioxide jet due to shock passage, as indicated by changes in the shape of the mean concentration contours, suggests that the baroclinic torque mechanism does not play a significant role in that case.

It can be noted that the density difference between the jet and air coflow, at a given downstream location, is less for the carbon dioxide jet than the corresponding helium jet owing to the molecular weight of air being much closer to that of carbon dioxide than that of helium. A value of the overall density gradient in the jet can be defined as $\Delta\rho/\delta_{5\%} \equiv (\rho_{cl} - \rho_{air})/\delta_{5\%}$, where ρ_{cl} and where ρ_{air} are, respectively, the average centerline jet density and the density of the air coflow and where $\delta_{5\%}$ is the jet width based on the 5% jet concentration contour. The magnitude of $\Delta\rho/\delta_{5\%}$ for the helium jet exceeds that of the carbon dioxide jet by factors of roughly 1.9 and 2.6, respectively, for the normalized downstream jet locations of $x/h = 29.6$ and 53.2. At the same time, the pressure rise across the shock wave, expressed as $\Delta p/p$, is more than twice as large for the $M_s = 1.4$ shock than for the $M_s = 1.2$ shock. The product of the overall density gradient and the shock pressure rise, $(\Delta\rho/\delta_{5\%})(\Delta p/p)$, is suggestive of the magnitude of the rate of baroclinic vorticity production for a given jet/shock combination. This parameter relates to the right-hand-side first term of the vorticity transport equation

$$\frac{\boldsymbol{D}(\omega/\rho)}{\boldsymbol{D}t} = \frac{\nabla\rho \times \nabla p}{\rho^3} + \frac{(\omega \cdot \nabla)\boldsymbol{u}}{\rho} \tag{7}$$

The absolute values of the parameter $(\Delta\rho/\delta_{5\%})(\Delta p/p)$ at $x/h = 29.6$ and 53.2 for the carbon dioxide jet, with a shock strength of $M_s = 1.4$ (Fig. 7), are comparable to those of the helium jet with a shock strength $M_s = 1.2$ (Fig. 4). Because in this study the jet is turbulent, the gradient of density is locally distributed in random directions. In addition, the thickness of the shock wave is not precisely known. Thus, the accurate estimation of the magnitude of the baroclinic torque is difficult. However, the sign of the quantity $\Delta\rho/\delta_{5\%}$, which plays an important role in the generation of vorticity, is clearly not the same for the light and heavy jets considered here. That vortical features appear to be generated only for the helium jet, and not for the carbon dioxide jet, suggests that the effects of baroclinic vorticity (which is necessarily of opposite sign in the helium jet vs the carbon dioxide jet) on jet structure and mixing are fundamentally different in a light jet vs a heavy jet.

These numerical results are qualitatively consistent with recent experiments,[22] which have also shown that shock passage in a helium jet can generate secondary vortical structure not produced by shock passage in a constant-density jet.

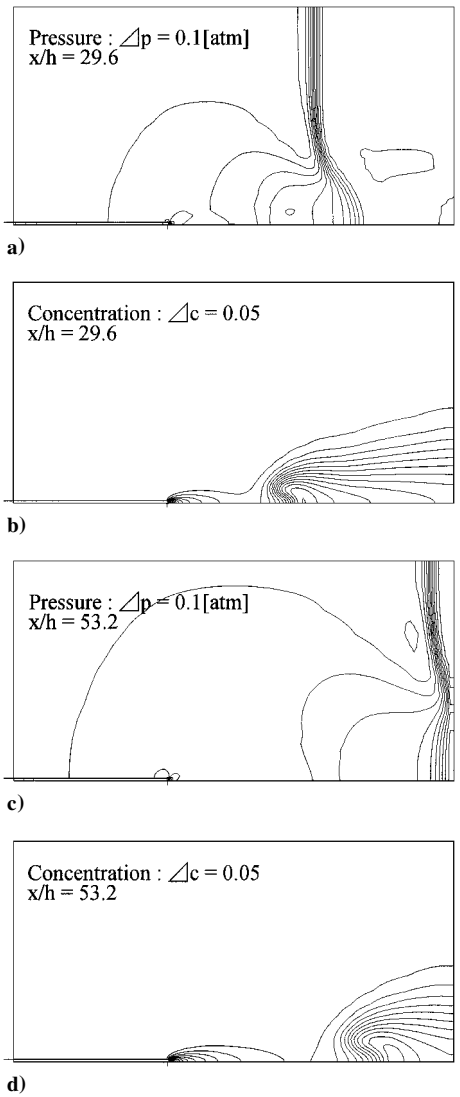

Fig. 5 Pressure and concentration contours for the interaction of a normal shock wave with a turbulent helium jet; shock propagation is from left to right with strength M_s = 1.4.

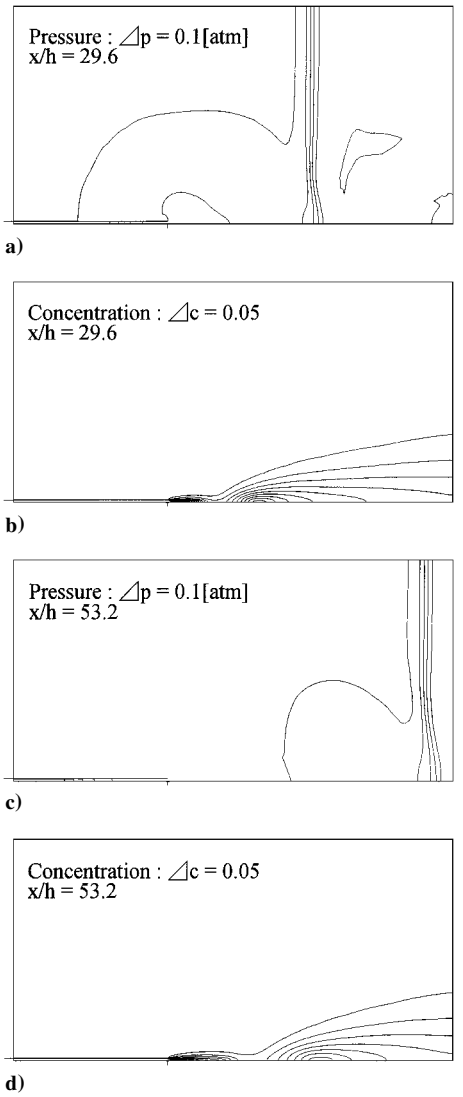

Fig. 6 Pressure and concentration contours for the interaction of a normal shock wave with a turbulent carbon dioxide jet; shock propagation is from left to right with strength M_s = 1.2.

Mean Jet Mixed Fluid Concentration

The concentration fields for the turbulent, planar jets with and without shock interaction were postprocessed to determine the average concentration in a given region of jet fluid, from which quantitative changes in jet mixing could be estimated. An average jet concentration was defined based on the area enclosed bounded by the 1% jet fluid concentration level by the following formula:

$$\bar{c} = \frac{\int_s c\,\mathrm{d}A}{\int_s \mathrm{d}A} \Rightarrow R_c = \frac{\bar{c}_{\text{with shock}}}{\bar{c}_{\text{without shock}}} \tag{8}$$

where c is the mole fraction of jet fluid and S indicates the region enclosed by the 1% jet fluid concentration level. The mean jet concentrations were obtained by computing the average concentrations for the regions behind the shock wave. For a shock strength of $M_s = 1.2$ the streamwise extent of this region was fixed at 21.2 and 39.1 jet nozzle heights for normalized shock positions of $x/h = 29.6$ and 53.2, respectively. For the $M_s = 1.4$ case the corresponding values were 17.3 and 31.1. These values are based on the distance between the shock position x_s and the location $x_f = x_s V_f / V_s$, where V_s is the shock propagation velocity and V_f the velocity of the gas behind the shock. The distance $x_s - x_f$ approximately corresponds to the distance from the shock wave to the pinched-off region of the jet. To allow for quantitative comparison of the mean jet concentration between jets with and without shock interaction, the streamwise extent of the regions over which Eq. (8) was evaluated for the unshocked jets was larger than that for the corresponding cases with shock wave interaction. This accounts for the shortening of the jet due to convection downstream of the shock discussed earlier. For the region immediately behind the shock, by taking the velocity in the jet to be negligible compared with the convection velocity behind the shock, the amount of this contraction can be shown to be equal to the density ratio across the shock wave, ρ_2/ρ_1.

The computed change in mean concentration for the air, helium, and carbon dioxide jets with and without shock interaction are shown in Table 1. The quantity R_c denotes the ratio of the average jet concentration for the case with shock interaction, as determined using Eq. (8), to that of the jet without the shock. The amount by which R_c is below unity is, thus, indicative of the degree of mixing enhancement. All jets shown exhibit some decrease in mean concentration, which reflects an increase in mixing, due to shock passage. The increase in mixing is more apparent in the nearer field of the jets ($x/h \approx 29.6$), than for the shock locations farther downstream. As baroclinic torque effects are effectively absent in the air jet cases and, based on the results of the preceding section, appear to not be significant for the carbon dioxide cases, any increase in mixing/decrease in mean concentration appears to be due essentially to changes in the convective flowfield brought about by shock passage.

The most substantial change in mixing occurs for the helium jet. For the stronger ($M_s = 1.4$) shock, the mean concentration decreases by as much as 30% at the normalized location $x/h = 29.6$ after shock passage compared with the baseline turbulent jet. For the weaker ($M_s = 1.2$) shock, the corresponding amount of mixing enhancement is approximately 22%. In both cases the mixing enhancement

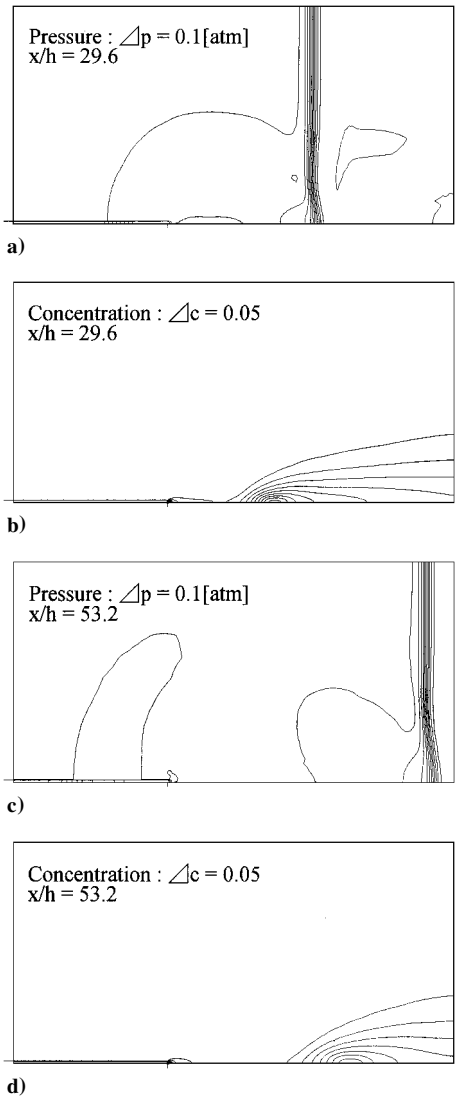

Fig. 7 Pressure and concentration contours for the interaction of a normal shock wave with a turbulent carbon dioxide jet; shock propagation is from left to right with strength $M_s = 1.4$.

Table 1 Normalized average jet fluid concentration

M_s	x/h	R_c
	Air	
1.2	29.6	0.862
1.2	53.2	0.887
1.4	29.6	0.858
1.4	53.2	0.886
	He	
1.2	29.6	0.779
1.2	53.2	0.829
1.4	29.6	0.697
1.4	53.2	0.774
	CO_2	
1.2	29.6	0.851
1.2	53.2	0.878
1.4	29.6	0.850
1.4	53.2	0.880

is less pronounced with increasing downstream distance. This is consistent with the baroclinic torque mechanism, which becomes weaker as the density gradient between the jet fluid and the coflowing airstream also decreases with downstream distance. The mixing enhancement for the helium jet is qualitatively consistent with the experimental result reported by Hermanson and Cetegen.[22] They measured a decrease in mean jet fluid concentration in an axisymmetric helium jet of nearly 30% at a downstream distance of 30 jet nozzle diameters after passage of an $M_s = 1.45$ shock. The regions over which the jet fluid concentration was averaged in that work were different in streamwise extent from those used in the current study.

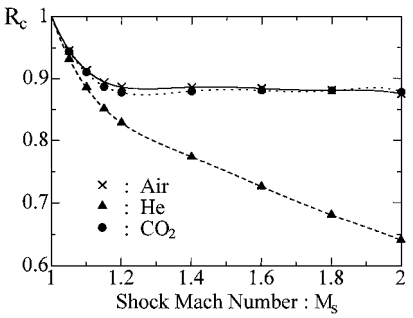

Fig. 8 Change in normalized average jet fluid concentration due to shock passage for turbulent helium, air, and carbon dioxide jets.

The change in average jet fluid concentration due to shock passage for the three jets is compared graphically in Fig. 8. In all cases shown here the shock is located at $x/h = 53.2$. The marked increase in mixing for the helium jet, as indicated by the drop in average normalized jet fluid concentration, can be seen in the figure. Compared to the helium jet, considerably less mixing enhancement is evident, for a given location and shock strength, for the air and carbon dioxide jets, where the effects of baroclinic torque are either absent (as in the case of air) or of the opposite sign (as in the case of carbon dioxide). This result is also qualitatively consistent with the experiment.[22]

Summary

A numerical study of the interaction of turbulent, planar air, helium, and carbon dioxide jets with weak normal shock waves was conducted. The numerical model was based on a time-dependent, N–S approach and employed a two-equation (q–ω) turbulence model. The shock waves were of strength $M_s = 1.2$ and 1.4, and the computational domain extended 60 nozzle heights downstream of the jet exit.

The helium jet exhibits a change in behavior due to shock propagation not apparent for the air and carbon dioxide jets. For the helium jets, the mean concentration contours suggest the generation of a vortex-like region centered on the jet centerline due to shock passage, consistent with the results of recent experiments. This vortical structure becomes more apparent for the higher shock strength, and is consistent with the expected vorticity generation due to the action of baroclinic torque. Such structure is not apparent for the case of the turbulent air jet, again consistent with experiment. The carbon dioxide jet also did not show the development of the vortical structure.

Consideration of the mean jet fluid concentration in the region behind the shock wave shows an increase in mixing of up to 30% for the helium jet at normalized downstream distance of $x/h = 30$ for the stronger ($M_s = 1.4$) shock wave. The amount of mixing enhancement is somewhat less (22%) for the weaker ($M_s = 1.2$) shock. The amount of mixing enhancement decreases with increasing downstream distance from the nozzle exit, owing to the lower jet concentration ahead of the shock.

Noticeably less mixing enhancement is seen for both the air and carbon dioxide jets due to shock passage, amounting to less than 15% in all cases studied. For $M_s \geq 1.2$, the amount of mixing enhancement for these jets appears to be insensitive to the shock strength. The considerably smaller increase in mixing for the air jet compared to the helium jet is qualitatively consistent with experiment.

These results suggest that baroclinic vorticity, to the extent that it is operative in turbulent jets subject to shock passage, has a fundamentally different effect in jets lighter than the ambient air than in heavy jets.

References

[1] Hollo, S. D., Hartfield, R. J., and McDaniel, J. C., "Injectant Mole Fraction Measurements of Transverse Injection in Constant Area Supersonic Ducts," AIAA Paper 90-1632, 1990.

[2]Hermanson, J. C., and Winter, M., "Mie Scattering Imaging of a Transverse, Sonic Jet in Supersonic Flow," *AIAA Journal*, Vol. 31, No. 1, 1993, pp. 129–132.

[3]Marble, F. E., Hendricks, G. J., and Zukoski, E. E., "Progress Toward Shock Enhancement of Supersonic Combustion Processes," AIAA Paper 87-1880, 1987.

[4]Waitz, I. A., Marble, F. E., and Zukoski, E. E., "Investigation of Contoured Wall Jet Injector for Hypervelocity," AIAA Paper 91-2265, 1991.

[5]Jacobs, J. W., "Dynamics of Shock Accelerated Light and Heavy Gas Cylinders," *Physics of Fluids A*, Vol. 5, No. 9, 1993, p. 2239

[6]Haas, J. F., and Sturtevant, B., "Interaction of Weak Shock Waves with Cylindrical and Spherical Gas Inhomogeneities," *Journal of Fluid Mechanics*, Vol. 181, 1987, pp. 41–76.

[7]Cetegen, B. M., and Hermanson, J. C., "Mixing Characteristics of Compressible Vortex Rings Interacting with Normal Shock Waves," *Combustion and Flame*, Vol. 100, 1995, pp. 232–240.

[8]Hollingsworth, M. A., and Richards, E. J., "On the Sound Generated by the Interaction of a Vortex with a Shock Wave," Aeronautical Research Council Fluid Motion Subcommittee, ARC 18257, F. M. 2371, 1956.

[9]Dosanjh, D. S., and Weeks, T. M., "Interaction of a Starting Vortex as Well as a Vortex Street with a Traveling Shock Wave," *AIAA Journal*, Vol. 3, No. 2, 1965, pp. 216–223.

[10]Naumann, A., and Hermanns, E., "On the Interaction Between a Shock Wave and a Vortex Field, Noise Mechanisms," CP-131, AGARD, Vol. 23-1, 1973.

[11]Ibragim, N. A., Klimov, A. I., and Shugaev, F. V., "Interaction Between a Vortical Ring and a Shock Wave," *Fluid Dynamics*, Vol. 13, No. 5, 1978, pp. 785–787.

[12]Ribner, H. S., "Cylindrical Sound Wave Generated by Shock–Vortex Interaction," *AIAA Journal*, Vol. 23, No. 11, 1985, p. 1708.

[13]Ellzey, J. L., Picone, M., and Oran, E. S., "Interaction of a Shock with a Compressible Vortex," Naval Research Lab., Memorandum 6919, Washington DC, 1992.

[14]Debieve, J. F., and Lacharme, J. P., "A Shock-Wave/Free Turbulence Interaction," *Turbulent Shear Layer/Shock Wave Interactions*, edited by J. Delery, Springer-Verlag, Berlin, 1986.

[15]Hussaini, M. Y., Collier, F., and Bushnell, D. M., "Turbulence Alteration Due to Shock Motion," *Turbulent Shear Layer/Shock Wave Interactions*, edited by J. Delery, Springer-Verlag, Berlin, 1986.

[16]Waitz, I. A., Marble, F. E., and Zukoski, E. E., "Vorticity Generation by Contoured Wall Injectors," AIAA Paper 92-3550, 1992.

[17]Yang, J., Kubota, T., and Zukoski, E. E., "Analytical and Computational Investigation of Shock-Induced Vortical Flows," AIAA Paper 92-0316, 1992.

[18]Jacobs, J. W., "Shock-Induced Mixing of a Light Gas Cylinder," *Journal of Fluid Mechanics*, Vol. 234, 1992, pp. 629–649.

[19]Budzinski, J. M., "Planar Rayleigh Scattering Measurements of Shock Enhanced Mixing," Ph.D. Dissertation, California Inst. of Technology, Pasadena, CA, 1992.

[20]Huh, H., and Driscoll, J. F., "Shock-Wave-Enhancement of the Mixing and the Stability Limits of Supersonic Hydrogen–Air Jet Flames," *Twenty-Sixth Symposium (International) on Combustion*, Combustion Inst., Pittsburgh, PA, 1996, pp. 2933–2939.

[21]Hermanson, J. C., and Cetegen, B. M., "Mixing Enhancement of Non-Uniform Density Turbulent Jets Interacting with Normal Shock Waves," *Twenty-Seventh Symposium (International) on Combustion*, Combustion Inst., Pittsburgh, PA, 1998, pp. 2047–2053

[22]Hermanson, J. C., and Cetegen, B. M., "Shock-Induced Mixing of Non-homogeneous Density Turbulent Jets," *Physics of Fluids*, Vol. 12, No. 5, 2000, pp. 1210–1225.

[23]Coakley, T. J., "Turbulence Modeling Methods for the Compressible Navier–Stokes Equations," AIAA Paper 83-1693, 1983.

[24]Gutmark, E., and Wygnanski, I., "The Planar Turbulent Jet," *Journal of Fluid Mechanics*, Vol. 73, No. 3, 1976, pp. 465–495.

[25]Obayashi, S., Matsushima, K., Fujii, K., and Kuwahara, K., "Improvements in Efficiency and Reliability for Navier–Stokes Computations Using the LU-ADI Factorization Algorithm," AIAA Paper 86-0338, 1983.

[26]Chakravarthy, S. R., and Osher, S., "New Class of High-Accuracy TVD Schemes for Hyperbolic Conservation Laws," AIAA Paper 85-0363, 1985.

[27]Anderson, W. K., Thomas, J. L., and Van Leer, B., "A Comparison of Finite Volume Flux Vector Splitting for the Euler Equations," AIAA Paper 85-0122, 1985.

[28]Chen, C. J., and Rodi, W., *Vertical Turbulent Buoyant Jets*, Pergamon, Oxford, 1980.

K. Kailasanath
Associate Editor